

# Diagnostic value of endobronchial ultrasound image features: A specialized review

Xinxin Zhi<sup>1,2,3,\*</sup>, Junxiang Chen<sup>1,2,3,\*</sup>, Fangfang Xie<sup>1,2,3</sup>, Jiayuan Sun<sup>1,2,3</sup>, Felix J. F. Herth<sup>4</sup>

<sup>1</sup>Department of Respiratory Endoscopy, Shanghai Jiao Tong University, Shanghai, China; <sup>2</sup>Department of Respiratory and Critical Care Medicine, Shanghai Chest Hospital, Shanghai Jiao Tong University, Shanghai, China; <sup>3</sup>Shanghai Engineering Research Center of Respiratory Endoscopy, Shanghai, China; <sup>4</sup>Department of Pneumology and Critical Care Medicine, Thoraxklinik, University of Heidelberg, Heidelberg, Germany

## ABSTRACT

Endobronchial ultrasound-guided transbronchial needle aspiration (EBUS-TBNA) technology is important in the diagnosis of intrathoracic benign and malignant lymph nodes (LNs). With the development of EBUS imaging technology, its role in noninvasive diagnosis, as a supplement to pathology diagnosis, has been given increasing attention in recent years. Many studies have explored qualitative and quantitative methods for the three EBUS modes, as well as a variety of multimodal analysis methods, to find the optimal method for the noninvasive diagnosis using EBUS for LNs. Here, we review and comment on the research methods and predictive diagnostic value, discuss the existing problems, and look ahead to the future application of EBUS imaging.


**Key words:** endobronchial ultrasound, lymph node qualitative analysis, quantitative analysis, sonographic feature

## INTRODUCTION

Endobronchial ultrasound-guided transbronchial needle aspiration with the guidance of a convex array probe (CP-EBUS-TBNA) is a new technology developed in 2002 that can facilitate minimally invasive biopsy of intrathoracic lymph nodes (LNs).<sup>[1,2]</sup> EBUS-TBNA revolutionized intrathoracic disease diagnosis and lung cancer staging and is a pivotal procedure in invasive thoracic workup. In addition to the diagnosis and staging of lung cancer,<sup>[3,4]</sup> intrathoracic LN metastases,

and lymphomas, EBUS-TBNA also has a significant diagnostic value in benign intrathoracic LNs.<sup>[5,6]</sup> Through the ultrasound probe mounted on the front of the bronchoscope, the operator can observe morphological characteristics of LNs in real time and evaluate the nature of LNs before puncturing.

In clinical diagnosis of abnormal LNs, intrathoracic LNs are usually selected for biopsy based on abnormal

Access this article online	
Quick Response Code:	Website: www.eusjournal.com
	DOI: 10.4103/eus.eus_43_20

This is an open access journal, and articles are distributed under the terms of the Creative Commons Attribution-NonCommercial-ShareAlike 4.0 License, which allows others to remix, tweak, and build upon the work non-commercially, as long as appropriate credit is given and the new creations are licensed under the identical terms.

**For reprints contact:** WKHLRPMedknow\_reprints@wolterskluwer.com

**How to cite this article:** Zhi X, Chen J, Xie F, Sun J, Herth FJ. Diagnostic value of endobronchial ultrasound image features: A specialized review. *Endosc Ultrasound* 2021;10:3-18.

\*These authors contributed equally to this article

### Address for correspondence

Dr. Jiayuan Sun, Department of Respiratory Endoscopy, Department of Respiratory and Critical Care Medicine, Shanghai Chest Hospital, Shanghai Jiao Tong University, 241 West Huaihai Road, Shanghai 200030, China. E-mail: xkyjysun@163.com

**Received:** 2020-04-02; **Accepted:** 2020-06-10; **Published online:** 2020-07-21

computed tomography (CT) and/or position emission tomography (PET)-CT. Increased size or FDG uptake of LNs on CT or PET-CT can guide the selection of LNs to undergo EBUS-TBNA. In patients undergoing EBUS-TBNA, ultrasonographic features are suggested to be used to predict malignant and benign diagnoses.<sup>[7]</sup> Just as ultrasound doctors can distinguish the benign and malignant lesions by ultrasound images, bronchoscopists can use ultrasonographic features to judge the benign and malignant LNs during the process of EBUS-TBNA. EBUS imaging can guide the selection of LNs for biopsy as well as internal puncture site within the LN and biopsy efficiency. In addition, for EBUS-TBNA negative results or insufficient tissue volume, EBUS sonographic features have a good complementary diagnostic value.

EBUS has three modes including gray scale, blood flow Doppler, and elastography, which can display sonographic features of LNs [Figure 1]. Bronchoscopists often use qualitative method to evaluate the characteristics in clinical practice. A variety of quantitative methods for the three modes have emerged in recent years to reduce subjectivity of qualitative assessments. These methods are similar to those used in EUS and in other superficial LNs.<sup>[8]</sup> To form a clinically applicable evaluation system, researchers have developed various scoring systems for EBUS, but there is no comprehensive scoring system combining three modes at present. The purpose of this review is to systematically summarize and comment on the diagnostic value and research progress of EBUS imaging.

## GRAY SCALE MODE

Gray scale mode is the most traditional ultrasound mode and reflects morphological features including size, shape, echogenicity, margin, central hilar structure (CHS), nodal conglomeration, coagulation necrosis sign (CNS), and calcification. Every feature can be analyzed by its own qualitative methods. Sonographic features of gray scale mode in differentiating benign and malignant LNs are summarized in Table 1. Quantitative methods are applied in gray scale mode as well, which can reduce subjectivity.

### *Qualitative methods of gray scale mode*

#### Shape

LN shapes include round, oval, and triangular. Round and oval are defined as long-axis/short-axis ratio  $<1.5$  and  $\geq 1.5$ , respectively. LNs are recognized

as triangular if the operator can see three arms on sonography.<sup>[9]</sup> Wang Memoli *et al.* used draping shape in the study, but the shape of the LNs was based on the visual relationship of the long to short axis and was agreed on by the two bronchoscopists performing the procedure.<sup>[10]</sup> Rigorous objective measurements of the ultrasound image with the EBUS software or post-procedure calculations of long axis to short axis ratio to determine round or oval shape were not routinely performed, so the result may be more subjective. In other words, it is more applicable to general practice, as definitive size measurements can be cumbersome and time-consuming during the actual procedure.<sup>[10]</sup> Lin *et al.* used the shape of round or non-round, and non-round was defined as long axis / short axis ratio more than 1.5, or the LNs had other irregular shapes (such as a triangular shape).<sup>[11]</sup> Multiple studies have found that round shape is an independent predictor of malignant LNs.<sup>[11-13]</sup> Imai *et al.* defined long axis diameter to short axis diameter  $\geq 2$  as oval, but the results showed no significant differences between sarcoidosis and lung cancer.<sup>[14]</sup> Two studies mentioned triangle. Gogia *et al.* found that triangular-shaped LNs are a strong predictor of benign disease,<sup>[9]</sup> and Wang Memoli *et al.* found that round and oval LNs were more likely to be malignant than triangular LNs.<sup>[10]</sup> In studies about benign LNs, Dhooria *et al.* found that most of the LNs were oval rather than round in the study of differentiating tuberculosis from sarcoidosis, and this result correlates with other studies because there were no malignant LNs in this study.<sup>[15]</sup>

#### Size

When multiple LNs are seen at one LN station, the largest LN is usually sampled for biopsy.<sup>[12]</sup> The size of the LNs incorporates the long and short axes. The long axis is the maximum diameter of the largest section of the LN in gray scale images, and the short axis is the largest diameter perpendicular to the long axis. The short axis and long axis are measured as distances of two perpendicular directions for triangular-shaped LNs.<sup>[12]</sup> The boundary of the short axis is usually 10 mm, and a short axis  $>10$  mm correlates with malignancy. Some studies classified short axis as a specific value. Wang *et al.* found that short axis  $>1.42$  cm has the highest sensitivity and specificity in predicting malignancy.<sup>[13]</sup> Fujiwara *et al.* found that the size had a diagnostic accuracy of 76.4%, but logistic regression analysis revealed that round shape, distinct margin, heterogeneous echogenicity, and presence of CHS were independent predictive factors for metastasis, and not short axis.<sup>[12]</sup> Wang Memoli *et al.*

**Table 1. Summary of sonographic features for malignant lymph nodes prediction of gray scale mode**

Sonographic features	Sensitivity (%)	Specificity (%)	PPV (%)	NPV (%)	Accuracy (%)
Short axis >10 mm <sup>[9,11,12,17-19,26,47,51,54,59,74]</sup>	80.3 (49.3-96.8)	57.5 (14.3-80.9)	59.2 (35.2-89.0)	79.6 (53.9-90.8)	73.7 (38.2-89.0)
Round shape <sup>[9,11-13,17-19,26,47,54,59]</sup>	79.8 (16.0-95.9)	53.1 (21.0-98.9)	72.2 (50.5-95.8)	75.0 (36.6-94.1)	68.0 (54.6-90.8)
Heterogeneous echogenicity <sup>[11,12,17-19,21,26,47,51,54,59]</sup>	77.3 (25.5-99.0)	73.8 (16.5-100.0)	76.7 (52.6-100.0)	77.5 (16.5-94.4)	77.1 (56.1-83.9)
Distinct margin <sup>[9,11,12,17-19,21,26,51,54,59]</sup>	76.8 (11.6-100.0)	55.4 (12.0-92.6)	55.7 (32.5-87.7)	66.2 (28.6-100.0)	67.0 (41.8-81.1)
Absent of CHS <sup>[9,12,13,17-19,21,54,59]</sup>	87.4 (15.6-100.0)	57.5 (8.7-96.0)	61.7 (30.6-95.3)	80.2 (17.8-100.0)	60.6 (28.5-83.2)
Present of CNS <sup>[12,17,18,21,47,59]</sup>	25.8 (8.8-69.4)	92.3 (81.8-99.8)	78.7 (77.8-97.0)	67.9 (16.1-88.4)	69.5 (22.1-86.0)
Present of nodal conglomeration <sup>[13,21]</sup>	31.3 (27.5-35.1)	94.3 (92.0-96.6)	95.6 (94.7-96.4)	27.9 (19.5-36.3)	45.0 (37.8-52.1)
Echo intensity <sup>[17,19,51]</sup>	53.8 (21.0-96.9)	78.0 (10.1-78.5)	49.0 (29.5-73.3)	60.8 (49.4-89.4)	51.8 (34.4-69.1)
Present of calcification <sup>[17,21]</sup>	50.9 (2.3-99.4)	54.4 (8.7-100.0)	64.9 (29.7-100.0)	57.0 (16.3-97.7)	26.0 (17.9-34.1)

Data was presented as median (range). CHS: Central hilar structure; CNS: Coagulation necrosis sign; NPV: Negative predictive value; PPV: Positive predictive value

found that the likelihood of malignant LNs increases as size increases.<sup>[10]</sup> Most studies about size mainly refer to the short axis, and there are few studies about the long axis. Wang *et al.* found that a long axis >1.67 cm had higher diagnostic accuracy for predicting metastasis than the short axis, and 1.67 cm was similar to 1.70 cm of long axis in EUS study.<sup>[13,16]</sup>

### Echogenicity

Echogenicity includes homogeneous and heterogeneous echotexture in distribution, and anechoic, hypoechoic, isoechoic and hyperechoic in intensity, relative to the surrounding tissue.<sup>[17]</sup> Surrounding tissues such as mediastinal soft tissues are hyperechoic, and major vascular structures are hypoechoic.<sup>[10]</sup> A node is labeled as heterogeneous if there are multiple small areas of varying echogenicity,<sup>[15]</sup> excluding major vascular structures, which are hypoechoic. Heterogeneity is usually a predictor of malignant LNs.<sup>[12,18,19]</sup> Evison *et al.* proposed that only heterogeneity was a predictor of malignant LNs, which showed that 85% heterogeneous LNs were malignant, and the shape, margin, CHS, and CNS were not associated with malignancy.<sup>[20]</sup> However, some studies consider heterogeneity as a benign predictor. For example, Ayub *et al.* found that heterogeneity had an accuracy of 65.7% in predicting benign LNs.<sup>[21]</sup> Dhooria *et al.* found that heterogeneity is a predictor of tuberculosis because of necrosis, but in this study, the comparator was sarcoidosis, not malignancy.<sup>[15]</sup> Wang Memoli *et al.* found no statistical significance in echo intensity between malignant and benign LNs; only the size and shape were relevant.<sup>[10]</sup> Alici *et al.* found the diagnostic accuracy for hypoechoic appearance, short axis >10 mm, distinct margins, the absence of CHS, and calcification of metastatic LNs was low (34.1%–41.8%). Benign nodes, particularly those affected by anthracosis may show these features.<sup>[17]</sup>

### Margin

Margin is divided into distinct and indistinct. Distinct margin is defined as clear visualization of more than 50% of the margin with a high echoic border and is related to the expansion of malignant tumors. With rapid tumor growth, the surrounding lung tissue becomes a thin layer of collapse zone, and the boundary between tumor and lung tissue can be seen on ultrasound. Distinct margin usually predicts malignant LNs,<sup>[12,18]</sup> but can be a benign predictor as well. Ayub *et al.* found that the diagnostic accuracy of a distinct margin for benign LNs was 81.1%.<sup>[21]</sup> Wang Memoli *et al.* found no significant difference in margins between benign and malignant LNs.<sup>[10]</sup>

### Central hilar structure

CHS is a hyperechoic area within the LN and is either present or absent.<sup>[22]</sup> CHS can be further divided into central and eccentric. In general, CHS does not appear in malignant LNs, which may be caused by infiltration and compression of tumor tissue or necrotic tissue.<sup>[23]</sup> Absence of CHS is an independent predictor of malignant LNs.<sup>[12]</sup> Shafiek *et al.* found that the sensitivity of CHS absence in diagnosing malignancy was as high as 99%, and the negative predictive value (NPV) was 90%.<sup>[19]</sup> In Wang's study about benign LNs, absence of CHS can predict sarcoid nodes, while the presence can indicate lymphadenitis.<sup>[22]</sup>

### Nodal conglomeration

Nodal conglomeration is defined as multiple LNs in a single LN station. Wang Memoli *et al.* recorded the number of LNs as single or multiple, but did not perform statistical analysis.<sup>[10]</sup> Some studies divided nodal conglomeration into clustered formation and matting. Clustered formation is multiple LNs with well-demarcated margins.<sup>[13,22]</sup> Matting indicates multiple LNs fuse into one large LN due to the damage of lymph capsule, showing tumor spread beyond the LN

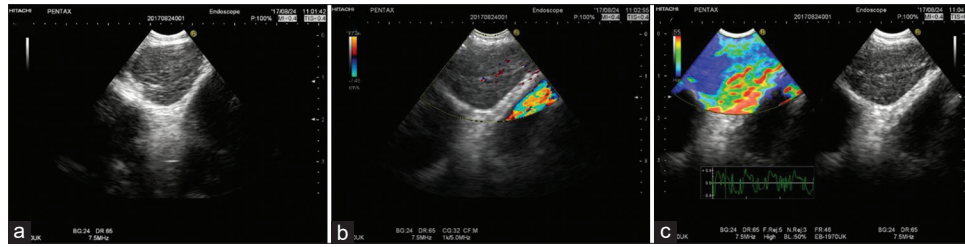


**Figure 1.** Schematic diagram of EBUS-TBNA and EBUS multimodal image. (a) EBUS gray scale image; (b) EBUS blood flow Doppler image; (c) EBUS elastography. EBUS-TBNA: Endobronchial ultrasound-guided transbronchial needle aspiration

capsule.<sup>[23]</sup> Nodal conglomeration has been reported to be a predictor of benign LNs, occurring in 27.5% of benign LNs and 8% of malignant LNs.<sup>[21]</sup> The presence of a clustered formation can predict sarcoidosis, while it was often absent in tuberculosis and reactive LNs.<sup>[22]</sup> However, present of matting is an independent predictor of malignant LNs.<sup>[13]</sup>

### Coagulation necrosis sign

CNS is a hypoechoic region within LNs, without blood flow.<sup>[12]</sup> This can be seen on EUS when detecting mediastinal LNs.<sup>[24]</sup> The typical CNS is one low hypoechoic region occupying majority of the LN, but multiple low echoic spots within the LN are recognized as heterogeneous echogenicity.<sup>[12]</sup> However, Alici *et al.* defined necrosis as cystic (an anechoic area within the LN without any Doppler acquisition) and coagulation (a hyperechoic area within the LN without shadowing).<sup>[17]</sup> Necrosis is usually a predictor of malignant LNs.<sup>[12]</sup> However, one study found that the diagnostic accuracy is only 22.1%, with no statistical difference between benign or malignant LNs.<sup>[21]</sup> In benign LNs, CNS usually appears in tuberculosis, and Dhooria *et al.* found that CNS occurred in 26.1% of tuberculosis, but only 3.3% of sarcoidosis cases,<sup>[15]</sup> which had significant statistical difference.

### Calcification

Calcification is a hyperechoic structure of various shapes with an acoustic shadow and can be further divided into absent, central, eccentric, and diffuse dotted calcification.<sup>[17]</sup> Fujiwara *et al.* did not include calcification as a significant echo feature because the incidence of calcification was rare in their experience with EBUS.<sup>[12]</sup> The specificity of calcification to identify benign and malignant LNs was 100% in one study, but the accuracy was only 17.9%.<sup>[21]</sup> Another study found that the accuracy of diagnosing calcification in the experimental group was only 34.1%.<sup>[17]</sup> In Wang's study, univariate analysis revealed that calcification was a predictor of malignancy, but

there was no statistical difference in multivariate regression.<sup>[13]</sup>

### Quantitative method of gray scale mode

Qualitative analysis about echogenicity is subjective, and thus Nguyen *et al.* used gray scale texture to quantitatively measure echogenicity. First-order gray scale texture features calculate the mean gray value within a region of interest (ROI) and depend on individual pixel values but not on their interaction with neighboring pixels.<sup>[25]</sup> Second-order gray scale texture features can reflect the color variance within ROI by measuring entropy, contrast, correlation, energy, and homogeneity [Figure 2]. Malignant LNs show a greater difference in the maximal and minimal pixel values, SEM pixel values, entropy, correlation, and a lower energy than benign LNs.<sup>[25]</sup>

### Comment on gray scale mode

The length of the short axis is related to the scan angle of the ultrasonic probe. Thus, the short axis is often limited by 1 cm rather than divided into a specific value. Operators can adjust the view to see the whole LN when it is too large and select the maximum section for the measurement. This problem can be reduced by wide-field imaging technology, which can capture a series of two-dimensional images by moving the probe, and then reconstruct and splice them into a continuous image.

## BLOOD FLOW DOPPLER

There are several kinds of blood flow Doppler. The application in EBUS field mainly includes energy Doppler reflecting intensity and color Doppler reflecting direction in the early stage. Currently, H-Flow and fine flow are commonly used due to its advantages of combining the two mentioned above.

### Qualitative methods of blood flow Doppler

Blood flow image evaluation includes blood flow volume and vascular distribution. Currently, there are

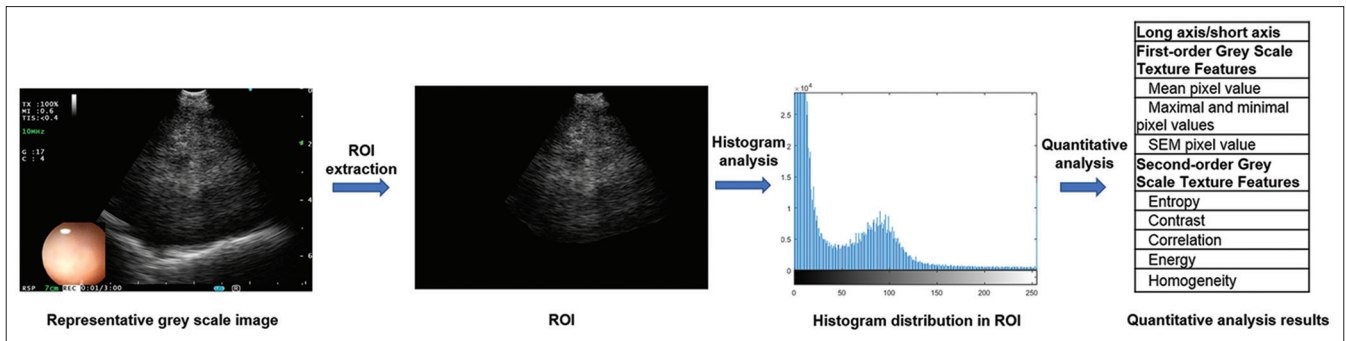


**Figure 2.** Diagram of quantitative method for EBUS gray scale image. The first-order gray scale texture features are mean pixel value within ROI reflecting echo intensity, and the second-order gray scale texture features mainly reflect echo homogeneity within ROI. EBUS: Endobronchial ultrasound; ROI: Region of interest

three qualitative methods reported to evaluate blood flow. The amount of blood flow was classified from 0 to 3 originating from breast cancer: Grade 0, no blood flow; grade 1, small amount of flow, one or two punctiforms or short rod-shaped of color flow signal; grade 2, medium amount of flow, one main vessel or a few small vessels could be found as a long strip of a curve; and grade 3, rich flow.<sup>[26,27]</sup> The results suggest no potential for predicting malignancy; grades 0 and 1 were not significantly different to grades 2 and 3.<sup>[26]</sup>

Wang *et al.* classified vascular patterns into three categories, according to blood flow distribution: (1) avascular, the absence of vascular signals within the LNs; (2) hilar, flow of signals that branches radially from the hilus, regardless of whether the signals originated from the central region or from the eccentric; (3) nonhilar, which includes central, capsular, and mixed (two or more types mixed from the hilar, central, and capsular). This classification method has a diagnostic accuracy of 79.69% in predicting LN metastasis, when defining ‘nonhilar vascular’ as malignant.<sup>[13]</sup> Tumor cells can produce tumor angiogenic factors, which stimulate angiogenesis and peripheral blood vessel growth. CHS are destroyed by tumor cells in the advanced stages of tumors. Therefore, malignant LNs are usually absent of CHS vascular, but benign LNs are usually not.<sup>[28]</sup>

Nakajima *et al.* combined vascular distribution with blood flow volume and graded vascular image patterns as follows: Grade 0, no blood flow or small amounts of flow; grade I, a few main vessels running toward the center of the LN from the hilum; grade II, a few punctiforms or rod-shaped flow signals or a few small vessels found as a long strip of a curve; grade III, rich flow, more than four vessels found with different diameters or twist- or helical-low signal. The blood flow from the bronchial artery (BA) toward the LN was also

recorded using Color Doppler imaging as a sign for BA inflow. When defining grades 0 and I as benign and grades II and III as malignant, the sensitivity, specificity, and accuracy were 87.7%, 69.6%, and 78.0%, respectively.<sup>[29]</sup> This method had pretty good diagnostic efficiency for that hilar vascular was proposed as a benign predictor in blood flow volume analysis.

#### *Quantitative methods of blood flow Doppler*

There have not been any studies about the application of quantitative methods for blood flow images in EBUS. Sun *et al.* developed a software copyright for the EBUS blood flow quantitative analysis system (China software copyright: 2019SR0069140), using the vascularity index (VI) and scattering index (SI) methods to quantitatively analyze blood vessels within LNs [Figure 3].

Blood flow quantitative methods are more developed in breast cancer, nasopharyngeal cancer, and laryngeal cancer. Zhou *et al.* studied the diagnostic value of the VI in 3D ultrasound in predicting metastases of cervical LNs. The terminal vessel branches of the tree-like framework within the tumor were counted one by one, by consensus of three sonographers, and then divided by the volume of the tumor to obtain the value of the VI. By analyzing the coordinates of the curve, the largest Youden’s index was 0.719, and the corresponding VI value was 4.4565. The accuracy of the curve coordinates as 85%, sensitivity was 95%, and the specificity was 75%. Therefore, VI for laryngeal cancer is an effective tool for predicting cervical LN metastasis.<sup>[30]</sup> Lee studied the application value of VI in LN metastasis of papillary thyroid carcinoma and the relationship among VI, VEGF, and microvessel density.<sup>[31]</sup> They found that VI was significantly correlated with microvessel density, but failed to show any significant correlations with LN

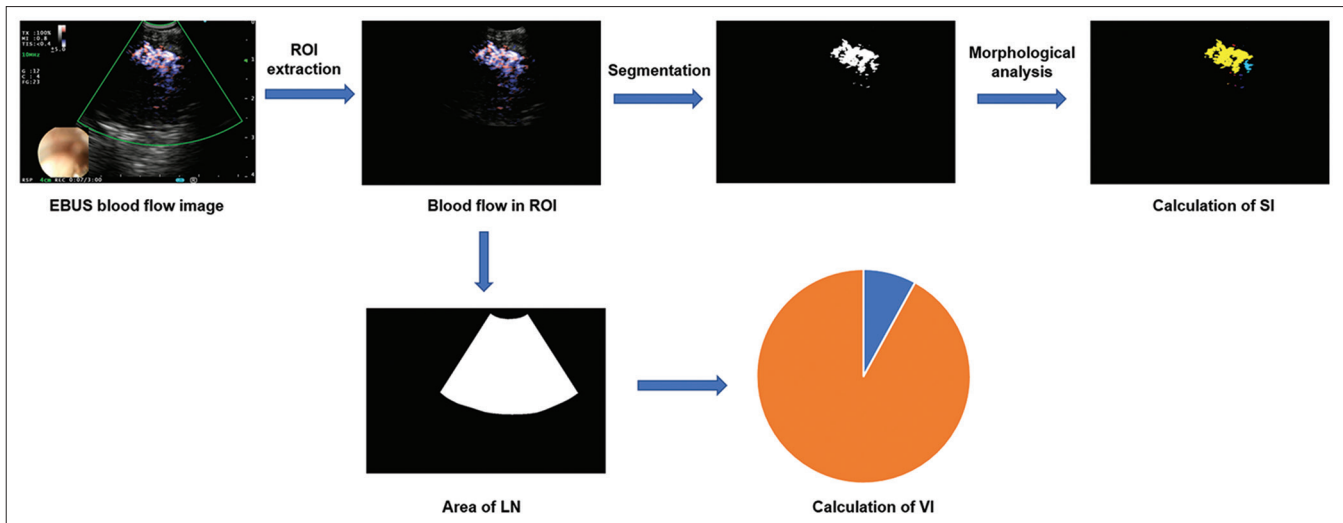


**Figure 3.** Diagram of quantitative method for EBUS blood flow image. The VI is defined as the number of pixels in the flow signals divided by the number of pixels in ROI. The SI is defined as the number of isolated flow signal units in ROI. VI: Vascular index; SI: Scattering index; ROI: Region of interest; LN: Lymph node

metastasis.<sup>[31]</sup> Kagawa *et al.* studied the relationship between the quantification of blood flow and the size of LNs in patients with cervical LNs metastasis of oral cancer and used VI and SI to analyze the largest section images of LNs. Isolated flow signal units of <3 pixels were excluded as noise signals. Researchers divided the LNs into four groups of different sizes and found that, for metastatic LNs, the VI was highest in Group 1, and decreased as size increased. The VI of benign LNs did not differ significantly among the four groups. For metastatic LNs, the SI increased as LN size increased and was significantly higher than that of benign LNs in Groups 2–4. Flow signal units are more scattered in larger metastatic LNs because the increased number of blood vessels produced by angiogenesis are displaced by the growth of tumor cells, forcing the blood vessels to move around or through tumor cells. A Doppler ultrasound image shows only one cut surface of an entire LN, and thus meandering blood vessels appear as scattered flow signal units. With tumor cell growth, the meandering of blood vessels increases. Therefore, SI representing the discontinuity of flow signals increases as LN size increases.<sup>[32]</sup> Quantitative methods can reduce the error caused by subjective factors, and its diagnostic value in EBUS is worth exploring.

#### *Comment on blood flow Doppler*

Blood flow volume grading method is not ideal,<sup>[26]</sup> and a new and effective method needs to be developed. Moreover, the combination of qualitative and quantitative methods may have greater application value and need further research.

## ELASTOGRAPHY

As a new ultrasound imaging technology, elastography can measure the degree of tissue deformation in gray scale mode and quantify tissue elasticity.<sup>[33,34]</sup> The colors related to hard tissue, intermediate state, and soft tissue are blue, green, and yellow/red, respectively.<sup>[35]</sup> Elastography was first applied to breast lesions,<sup>[36]</sup> and later used in prostate,<sup>[37]</sup> thyroid,<sup>[38]</sup> pancreas,<sup>[39]</sup> liver,<sup>[40]</sup> EUS,<sup>[41]</sup> and EBUS examinations,<sup>[42,43]</sup> to help distinguish benign and malignant LNs and lesions. In general, tumor tissue has more cells and blood vessels, so it has a harder texture than normal tissue.<sup>[44]</sup> In other words, the harder the tissue, the more likely it is malignant. Therefore, the principle of elastography is to reflect malignancy indirectly by measuring the hardness of tissue. In EBUS elastography, by comparing the elasticity of the target tissue and surrounding tissue, the scanned area can be reconstructed and converted into a color signal, which is superimposed on the B-mode imaging, and the B-mode image and elastography are displayed on the monitor at the same time. This section mainly describes the application methods of elastography in EBUS images, including qualitative and quantitative methods.

### *Qualitative methods of endobronchial ultrasound elastography*

#### *Three-score method*

Izumo *et al.* first classified elastography into three types: Type 1, predominantly non-blue (green, yellow, and red); Type 2, part blue, part non-blue (green, yellow, and red); and Type 3, predominantly blue.<sup>[45]</sup>

This method classified Type 1 as benign and Type 3 as malignant and was used by many subsequent studies.<sup>[18,46-50]</sup> Studies about qualitative methods of EBUS elastography are summarized in Table 2. Korrungruang *et al.* classified elastography into type 1 and non-type 1 for statistics,<sup>[48]</sup> and Hernández Roca *et al.* compared Types 1 and 2 with Type 3.<sup>[50]</sup> For type 1 LNs, a high NPV can reduce unnecessary puncture when rapid on-site evaluation (ROSE) shows adequate TBNA specimen and benign lymphocytes. Type 3 elastography can guide the rapid selection of LNs that need to be punctured. However, type 2 cannot differentiate benign and malignant, so this method may have limited clinical application value.

#### Four-score method

He *et al.*<sup>[51]</sup> used the four-score method of Furukawa *et al.*<sup>[52]</sup> in head and neck LNs: 1 point when over 80% of the section was green and yellow/red; 2 points when over 50% but <80% of the section was green and yellow/red; 3 points when over 50% but <80% of the section was blue; and 4 points when over 80% of the section was blue. This method defined points  $\geq 2.5$  as malignant and was used in central lung lesions later.<sup>[53]</sup> The results are listed in Table 2. The four-score method did not classify the cutoff as an integer value, and the percentage of color is difficult to accurately define in clinical operations, so this method has limited clinical significance.

#### Five-score method

Sun *et al.* divided elastography qualitative scores into five scores [Figure 4],<sup>[54]</sup> which comes from EUS elastography.<sup>[55]</sup> By classifying 1–3 as benign and 4–5 as malignant, Sun *et al.* found that the mean values of malignant and benign LNs were  $4.29 \pm 0.71$  and  $2.82 \pm 1.18$ , respectively, and the diagnostic accuracy was 83.82%. By comparing the diagnostic efficiency of single B-mode features, 5-score method, and mean gray value, 5-score method had the highest diagnostic accuracy.<sup>[54]</sup> Verhoeven *et al.* used two visual analog scale (VAS) scoring methods for visual scoring of the strain – the first method: 1, predominantly blue; 2, blue and green; 3, predominantly green; 4, green and red; and 5, predominantly red. The second method is a modified version of the Tsukuba score, a scoring system based on a combination of the visualized color and the pattern of the strain image: Score 1, strain is seen in the entire hypochoic area (the entire lesion is shown in green similar to the surrounding tissue); Score 2, strain is seen within most of the hypochoic area but

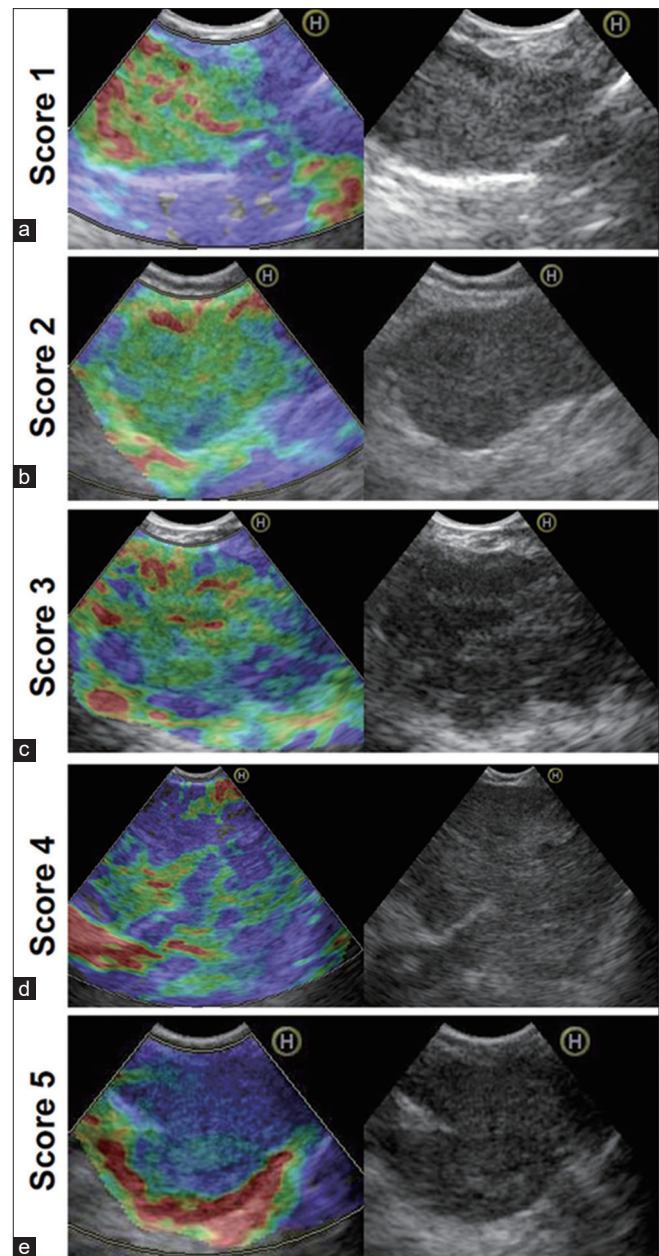


**Figure 4.** Representative appearance of the qualitative pattern analysis of EBUS elastography images.<sup>[54]</sup> (a) Score 1 (scattered soft, mixed green-yellow-red); (b) Score 2 (homogeneous soft, predominantly green); (c) Score 3 (intermediate, mixed blue-green-yellow-red); (d) Score 4 (scattered hard, mixed blue-green); (e) Score 5 (homogeneous hard, predominantly blue). EBUS: Endobronchial ultrasound

some areas show no strain (the lesion is a mixture of red, green, and blue); Score 3, strain appears only in the periphery, no strain in the center of the lesion (center of the lesion is blue, the periphery is green); Score 4, no strain is measured within the lesion (the entire lesion is shown in blue); Score 5, no strain is measured within the lesion nor in the surrounding tissues (the lesion and the surrounding tissues are blue); and Score X, typical artifact seen when blood vessels invade the LN. Red in the center of the surrounding vessel, green in the

**Table 2. Studies about qualitative methods of endobronchial ultrasound elastography**

Study	Study type	Method	Pathological result	Number of LNs	Sensitivity (%)	Specificity (%)	PPV (%)	NPV (%)	Accuracy (%)
Izumo <i>et al.</i> [45]	Retrospective	Three-score	LNs (22 adc, 5 Scc, 4 SCLC, 3 NSCLC, 8 nonpulmonary malignancies, 33 benign)	75	100	92.3	94.6	100	96.7
Lin <i>et al.</i> [18]	Retrospective	Three-score	Patients (30 Adc, 14 Scc, 8 SCLC, 4 other NSCLC, 2 esophageal cancer, 1 breast cancer, 1 oropharyngeal cancer, 1 tongue cancer, 1 spindle cell carcinoma, 7 sarcooidosis, 1 TB, 3 pneumoconiosis, 1 Wegener granulomatosis, 1 atypical lymphoid hyperplasia, 2 peribronchial cyst, 17 pneumonia)	206	90.6	82.6	71.6	94.7	85.2
Gu <i>et al.</i> [47]	Prospective	Three-score	LNs (20 Adc, 17 Scc, 17 SCLC, 10 NSCLC and 25 NSCLC-NOS, 44 benign)	133	100	65	85.7	100	88.7
Huang <i>et al.</i> [46]	Retrospective	Three-score	LNs (20 normal, 25 epithelioid granuloma lesions, 7 SCLC, 21 Adc, 2 Scc, 1 between the cytopathology of malignant tumor, 1 diffuse large B cell lymphoma and 1 carcinoid tumor)	78	96.43	86.67	87.10	96.30	91.38
Korrruang and Boonsarngsuk <sup>[48]</sup>	Prospective	Three-score	LNs (11 SCLC, 68 NSCLC, 15 metastasis, 2 lymphoma, 15 TB, 1 histoplasmosis, 1 silicosis, 7 reactive lymph node)	120	100	66.7	92.3	100	∖
Fournier <i>et al.</i> [49]	Prospective	Three-score	Patients (70 mediastinal-hilar adenopathies, 7 bronchopulmonary cancer, 8 sarcooidosis, 9 isolated mediastinal lymph node, 6 pulmonary cancer, 14 metastases of an extrapulmonary cancer)	217	87	68	80	77	∖
Hernández Roca <i>et al.</i> [50]	Prospective	Three-score	LNs (1 nonrepresentative lymph nodes, 18 malignant, 24 normal or benign)	43	73	92	86	81	∖
He <i>et al.</i> [51]	Retrospective	Four-score	LNs (12 Scc, 11 Adc, 9 SCLC, 10 low differentiation cancer, 26 benign)	68	76.9	85.7	85.7	76.9	82.3
He <i>et al.</i> [53]*	Retrospective	Four-score	Patients (11 Scc, 8 Adc, 14 SCLC, 3 low-differentiation cancer, 21 benign)	57	72.2	76.2	83.4	61.5	73.7
Sun <i>et al.</i> [54]	Prospective	Five-score	LNs (12 Adc, 5 Scc, 4 NSCLC-NOS, 13 SCLC, 1 lymphoma, 7 TB, 12 sarcooidosis, 14 nonspecific lymphadenitis)	68	85.71	81.82	83.33	84.38	83.82
Verhoeven <i>et al.</i> [56]	Prospective	VAS scoring	LNs (75 benign, 19 Adc, 15 Scc, 1 NSCLC NOS, 5 SCLC, 3 large cell neuroendocrine carcinoma, 2 invasive ductal carcinoma)	120	80	76	67	86	78
Verhoeven <i>et al.</i> [56]	Prospective	Modified version of the Tsukuba score	LNs (75 benign, 19 Adc, 15 Scc, 1 NSCLC NOS, 5 SCLC, 3 large cell neuroendocrine carcinoma, 2 invasive ductal carcinoma)	120	89	76	69	92	81
Trosini-Désert <i>et al.</i> [58]	Prospective	Five-score	LNs (18 Adc, 9 Scc, 7 NSCLC, 5 SCLC, 1 lymphoma, 2 breast cancer metastases, 1 pancreatic cancer metastases, 1 hepatocellular carcinoma metastases, 61 normal lymph node tissue, 2 TB, 3 sarcooidosis)	110	77	95	92	86	∖

\*This study was conducted on central lung lesions. Adc: Adenocarcinoma; Scc: Squamous cell carcinoma; SCLC: Small cell lung cancer; NSCLC: Non-SCLC; TB: Tuberculosis; NSCLC-NOS: NSCLC not otherwise specific; EBUS: Endobronchial ultrasound; NPV: Negative predictive value; PPV: Positive predictive value; VAS: Visual analog scale; LNs: Lymph nodes



vicinity. The first VAS scoring method classified 1–2 points as malignant and 3–5 points as benign. And, the second classified scores 4–5 as malignant and scores 1–3 as benign.<sup>[56]</sup> Trosini-Désert *et al.* used a color score originating from pancreatic masses: Score 1 was assigned when the image showed a homogenous soft tissue area (green) corresponding to normal tissue; score 2 was when the image indicated heterogeneous soft tissue (green, yellow, and red) corresponding to fibrosis or inflammatory tissue; score 3 was when the image displayed mixed colors or a honeycombed elastography pattern indicative of mixed hard and soft tissue making the interpretation difficult; score 4 was when the image displayed a small soft (green) central area surrounded by mainly hard (blue) tissue corresponding to a malignant hypervascularized lesion; and score 5 was assigned to lesions representing mainly hard (blue) tissue with areas of heterogeneous soft tissue (green and red) representing zones of necrosis in an advanced malignant lesions.<sup>[57]</sup> Score 3 was an indeterminate color, and in pancreatic masses, score 1–2 was considered as benign and 3–5 as malignant; but in EBUS elastography, classifying 1–3 as benign and 4–5 as malignant may achieve the best diagnostic performance.<sup>[58]</sup> In clinical practice, setting the NPV of elastography parameters to 100% is important to not miss a malignant lesion. Scoring <3 as benign can achieve an NPV of 100% for malignancy.<sup>[58]</sup> The modified Tsukuba score combines with the hardness of surrounding tissues, which may be not suitable for LNs images that are too large to see the boundary. Compared with the three or four-score method, the five-score method is more detailed and comprehensive in dividing colors.

### *Quantitative methods of endobronchial ultrasound elastography*

#### **Strain ratio**

Qualitative methods are usually affected by subjective factors, and more objective quantitative methods are needed. The largest possible area of the node is outlined from the superimposed elastography image, and the same procedure was performed on a similar-sized area that was surrounded by apparently normal tissue. SR is the strain of surrounding tissue to LN. Studies about SR method in EBUS elastography are shown in Table 3.<sup>[48,51,56,58,59]</sup> Hernández Roca *et al.*<sup>[50]</sup> found that the best cutoff value of SR was 4, and the corresponding area under the curve (AUC) was 0.75. The calculation of SR requires the presence of surrounding mediastinal tissue and avoiding large blood

vessels, but many elastic images of LNs fail to meet this requirement. The measurement of SR correlates with the depth of ROI and reference area, since different depths of region with the same hardness may appear different strain. Furthermore, the results also varied with the selection of control areas. The optimal cutoff value of SR showed large variations between different studies, ranging from 4 to 32.07.<sup>[50,51]</sup> Compared with frequency histogram and stiff area ratio (SAR), SR is a more variable parameter.<sup>[60]</sup>

#### **Stiff area ratio**

SAR is the ratio of pixels in the blue area to the area of target LN. Diagnostic values of SAR in predicting malignancy are shown in Table 3.<sup>[61–63]</sup> Ma *et al.* used the concept of blue color proportion, that is, the pixel value of the blue area divided by the pixel value of the entire LN area.<sup>[63]</sup> Mao *et al.* defined blue pixels that range from 145 to 180 in the HSV color model as hard areas.<sup>[64]</sup> Hernández Roca *et al.* defined the color density of 0–49 in RGB color model as blue, which is a hard area, finding that malignant LNs had a higher proportion of blue pixels (66% *vs.* 32.5%,  $P = 0.016$ ). When the value is 52, the AUC is 0.87.<sup>[50]</sup> In Abedini's study, the results showed that a significant correlation when SAR was used as the predictor of malignancy or anthracosis.<sup>[61]</sup> Nakajima *et al.* found that there was no statistical difference of benign and malignant LNs SAR in the *ex vivo* surgical samples, with a malignant mean SAR of 0.300 and a benign mean SAR of 0.269.<sup>[62]</sup> Elastography cannot visualize the absolute value of tissue elasticity. It can only show the stiffness of the LN area relative to the surrounding tissue. The external environment is different from the internal environment, and it is difficult to cover the entire LN area, so results will vary, indicating that the SAR method may be not appropriate *in vitro*.<sup>[62]</sup>

#### **Strain histogram**

The strain histogram is the average strain value in the selected area, which represents average tissue elasticity. In the histogram, the X-axis represents the elastic value between 0 and 255 (each value is represented by the pixel color), where 0 is the hardest and 255 is the softest, and the Y-axis represents the number of pixels for each value.<sup>[65]</sup> Table 3 lists some studies about EBUS strain histogram.<sup>[56,58]</sup> Hernández Roca *et al.*<sup>[50]</sup> reported that the average color dispersion of malignancy was lower than that of benign (48.8 *vs.* 94.8). When the average dispersion of LNs was 61, the diagnosis efficacy was the best, with an AUC of 0.83. Verhoeven *et al.* found that the strain histogram

Table 3. Studies about quantitative methods of elastography

Study	Study type	Method	Pathological result	Number of LNs	Cut-off	Sensitivity (%)	Specificity (%)	PPV (%)	NPV (%)	Accuracy (%)
He et al. <sup>[51]</sup>	Retrospective	SR	LNs (12 Scc, 11 Adc, 9 SCLC, 10 low differentiation cancer, 26 benign)	68	32.07	88.1	80.8	88.1	80.8	85.3
Rozman et al. <sup>[59]</sup>	Prospective	SR	Patients (14 Adc, 8 Scc, 3 SCLC and 2 NSCLC, 2 post-tuberculous changes, 2 pneumonia/lung abscesses, 1 sarcooidosis and 1 infectious mononucleosis)	80	8	88.24	84.78	81.08	90.7	86.25
Korrunguang and Boonsarngsuk <sup>(48)</sup>	Prospective	SR	LNs (11 SCLC, 68 NSCLC, 15 metastasis, 2 lymphoma, 15 TB, 1 histoplasmosis, 1 silicosis, 7 reactive lymph node)	120	15.3	87.5	79.2	94.4	61.3	∕
Verhoeven et al. <sup>[56]</sup>	Retrospective	SR	LNs (75 benign, 19 adenocarcinoma, 15 squamous cell carcinoma, 1 NSCLC NOS, 5 small cell lung carcinoma, 3 large cell neuroendocrine carcinoma, 2 invasive ductal carcinoma)	120	1.67	47	84	64	72	70
Trosini-Désert et al. <sup>[58]</sup>	Prospective	SR	LNs (56 nonmalignant, 42 malignant)	98	5.3	86	73	71	87	∕
Nakajima et al. <sup>[62]</sup>	Retrospective	SAR	Patients (14 lung cancer, 6 extrathoracic malignancies, 1 benign adenopathy)	49	0.311	81	85	∕	∕	∕
Abedini et al. <sup>[61]</sup>	Prospective	SAR	Patients (10 sarcooidosis, 1 TB, 5 reactive, 2 LC, 5 Adc, 1 metastatic carcinoma, 1 NSCLC, 1 mucinous cystadenoma)	69	0.36	80	85	80	85	83
Mao et al. <sup>[64]</sup>	Retrospective	SAR	LNs (12 Adc, 5 Scc, 4 NSCLC, 13 SCLC, 1 lymphoma, 7 TB, 12 sarcooidosis, 14 nonspecific lymphadenitis)	68	0.48	82.86	81.82	82.86	81.82	82.35
Ma et al. <sup>[63]</sup>	Retrospective	BCP	LNs (17 Adc, 2 Scc, 9 SCLC, 9 poorly differentiated carcinoma, 2 intestinal metastasized lung carcinoma, 22 normal lymphatic tissue, 14 inflammatory exudation, 2 bacterial infection, 2 noncaseating granulomas sarcooidosis)	79	36.7%	92.3	67.5	∕	∕	78.5
Trosini-Désert et al. <sup>[58]</sup>	Prospective	Strain histogram	LNs (18 Adc, 9 Scc, 7 NSCLC, 5 SCLC, 1 lymphoma, 2 breast cancer metastases, 1 pancreatic cancer metastases, 1 hepatocellular carcinoma metastases, 61 normal lymph node tissue, 2 tuberculosis, 3 sarcooidosis)	110	74.3	73	92	86	84	∕
Verhoeven et al. <sup>[56]</sup>	Retrospective	Strain histogram	LNs (75 benign, 19 Adc, 15 Scc, 1 NSCLC-NOS, 5 small cell lung carcinoma, 3 large cell neuroendocrine carcinoma, 2 invasive ductal carcinoma)	120	78	93	75	69	95	82
Sun et al. <sup>[54]</sup>	Retrospective	Mean gray value	LNs (12 Adc, 5 Scc, 4 NSCLC-NOS, 13 SCLC, 1 lymphoma, 7 TB, 12 sarcooidosis, 14 nonspecific lymphadenitis)	68	192.32	91.43	72.73	78.05	88.89	82.35
Mao et al. <sup>[64]</sup>	Retrospective	Mean hue value	LNs (12 Adc, 5 Scc, 4 NSCLC, 13 SCLC, 1 lymphoma, 7 TB, 12 sarcooidosis, 14 nonspecific lymphadenitis)	68	126.28	85.71	75.76	78.95	83.33	80.88

Adc: Adenocarcinoma; Scc: Squamous cell carcinoma; SCLC: Small cell lung cancer; NSCLC: Non-SCLC; TB: Tuberculosis; NSCLC-NOS: NSCLC not otherwise specific; EBUS: Endobronchial ultrasound; SR: Strain ratio; SAR: Stiff area ratio; BCP: Blue color proportion; LNs: Lymph nodes

is the best method compared to the SR and two other qualitative methods.<sup>[56]</sup>

### Mean gray value

After performing a pixel-by-pixel subtraction of the gray scale image from the elastography image, the matrix of red, green, and blue values obtained from subtraction can be transformed into a matrix of gray tone, and these values vary from 255 (all blue pixels) to 0 (all red pixels). The mean gray value is the ration of sum gray to number of points, which was used in breast cancer.<sup>[66]</sup> The average gray values of malignant and benign LNs in Sun's study were  $199.11 \pm 5.64$  and  $169.52 \pm 47.31$ , respectively ( $P < 0.01$ ),<sup>[54]</sup> and the software copyright of the EBUS elastography quantitative analysis system (China software copyright: 2015SR191866) has been developed.

### Mean hue value

The mean hue value is defined as the mean value of hue within an ROI, using the HSV color model, which was used for EUS research before.<sup>[67,68]</sup> Mao *et al.* used this method for EBUS elastography quantitatively, showing a worse diagnostic value than SAR in differentiating intrathoracic LNs.<sup>[64]</sup>

### Comment on elastography

Elastography can guide the selection of LNs for biopsy, the localization of malignant components within LNs,<sup>[69,70]</sup> and can be used as a ROSE technique for the diagnosis of non-small cell lung cancer (NSCLC). Elastography mainly reflects the hardness of tissue, so fibrosis within benign LNs and central necrosis within malignant LNs may influence the accuracy of elastic evaluation.<sup>[18]</sup> Fibrosis in sarcoidosis may show a blue pattern<sup>[71]</sup> and cause false-positive results, as well as calcification in pneumoconiosis LNs. In Abedini's study, with the exclusion of anthracosis nodes from analysis, the statistical difference between malignant and non-malignant (original  $P = 0.032$ ) was more significant ( $P < 0.001$ ).<sup>[61]</sup> Sun *et al.* found that tuberculosis and sarcoidosis LNs were stiffer than non-specific inflammation LNs due to the presence of epithelioid granulomas. False-negative results appeared in small cell lung cancer and lymphoma, and false-positive results appeared in nonspecific inflammation and tuberculosis.<sup>[54]</sup>

Elastography usually has better diagnostic value than a single gray scale feature.<sup>[54,59]</sup> He *et al.* found the diagnostic accuracy of distinct margins, homogenous,

hypochoic, no air-bronchogram, and elastography score in central lung lesions were 71.9%, 63.2%, 71.9%, 70.2%, and 73.7%, respectively.<sup>[53]</sup> However, elastography is easier to vary due to breathing exercises and adjacent vascular pulsations compared with gray scale and blood flow image. Hence, a representative elastography image should be selected from frames with good repeatability of dynamic recording under a relatively stable pressure curve or amplitude to reduce the bias. As the developing of neural network, it has been used in EUS and pancreatic mass elastography,<sup>[68,72]</sup> and can also be used in EBUS elastography, with automatic selection of representative images from videos, to achieve more objective results.

## ASSOCIATION OF ENDOBRONCHIAL ULTRASOUND IMAGE FEATURES AND PREDICTIVE TOOLS

The clinical application of EBUS sonographic features requires certain criteria. To explore the best diagnostic efficiency, some researchers combined several features and formulated scoring systems. Similar mathematical models can be seen with breast cancer.<sup>[73]</sup> Wang *et al.* found that at least two of the features (presence of matting, nonhilar vascular pattern perfusion, absence of CHS, and round shape) can achieve the best performance in predicting malignancy.<sup>[13]</sup> In differentiating benign LNs, Wang *et al.* found that at least four sonographic features from five categories (short axis  $>1$  cm, absence of CHS, distinct margin, presence of clustered formation, and presence of nonhilar perfusion) can achieve the optimal diagnostic efficiency in predicting sarcoid nodes, as well as two sonographic features (presence of necrosis sign and absence of clustered formation) in predicting tuberculous nodes, and at least two sonographic features of the three categories (presence of CHS, absence of clustered formation, and presence of hilar perfusion or avascular) in predicting reactive lymphadenitis.<sup>[22]</sup>

Trosini-Désert *et al.* combined colorimetric scores with LN diameter: colorimetric score 1 or 2 considered benign; colorimetric score 3 and diameter  $<13.8$  mm considered benign; and colorimetric score 4 and average elasticity  $<54$  considered malignant, which provided a sensitivity and specificity of 100% for LNs classified by one of these three rules.<sup>[58]</sup> The diagnostic accuracy in combing the four features (oval, indistinct margins, homogenous echogenicity, and absence of CHS) with

SR was 90.9% reported by Fujiwara *et al.*, which was higher than a single method.<sup>[74]</sup>

Shafiek *et al.* retrospectively analyzed 208 LNs and constructed a predictive system using five features including distinct margin, round shape, short axis  $\geq 10$  mm, heterogeneous echogenicity, and absence of CHS. The former three features were scored 1 point, and the latter two 1.5 points. In prospective verification of 65 LNs, the sensitivity and specificity of a sum score  $>5$  points were 78% and 86%, respectively. Among them, the absence of CHS, round shape, and size were significantly correlated with malignant LNs.<sup>[19]</sup>

Schmid-Bindert *et al.* developed a scoring model by retrospectively analyzed six features, including shape, margin, echogenicity, CHS, short axis, and blood flow. Researchers found that if the presence of 3–6 positive variates was seen as high risk, and 1–2 positive variates as low risk, the odds ratio for malignancy was 15.5 (95% CI: 3.631–66.173). The feasibility of the EBUS ultrasound standard lies in the NPV. When  $\leq 2$  features were present, the probability of malignancy was only 5%.<sup>[26]</sup>

Alici *et al.* retrospectively analyzed the echogenicity (anechoic, hypoechoic, isoechoic, or hyperechoic), echo homogeneity, shape, size, margin, necrosis, calcification, and CHS of 1,051 LNs. An algorithm on whether to sample LNs was constructed first in the experimental group, and then a modified algorithm was applied in the study group. The algorithm had sensitivity, specificity, positive predictive value (PPV), NPV, and accuracy of 100%, 51.2%, 50.6%, 100%, and 67.5%, respectively.<sup>[17]</sup>

Evison *et al.* investigated whether LNs with negative EBUS-TBNA results in lung cancer patients require further surgical staging. A risk model was constructed by three independent predictors (echogenicity, SUV, and SUV ratio) and was divided into low-risk group ( $\leq 1$  point) and high-risk group ( $\geq 2$  points). The NPV of the model in the modeling set and the validation set were 99.3% (95% CI: 96.1%–99.6%) and 97.9% (95% CI: 92%–99.6%), respectively. During the staging of lung cancer, for LNs with negative EBUS-TBNA results, this model can guide which patients need further staging and which can be treated directly.<sup>[20]</sup> Gu *et al.* constructed a scoring model using features including size, shape, heterogeneity, and qualitative elastography method. When 3–4 was classified as high

risk and 1–2 as low risk, the odds ratio for malignancy was 9.44 (95% CI: 3.99–22.32;  $P < 0.0001$ ), and the combined model was superior to elastography alone.<sup>[47]</sup>

## INTRA- AND INTEROBSERVER AGREEMENT

To study the consistency of ultrasound features within and between assessors, many studies use consistency assessment methods. Intraobserver consistency is defined as the difference of two assessments by the same assessor. Interobserver consistency is defined as differences between two or more evaluators and is usually assessed by means of Cohen's kappa ( $k$ ).  $k$  values range from 0 (no agreement other than what would be expected by chance) to 1 (perfect agreement).  $K$  values  $>0.81$  are considered as perfect agreement; 0.61–0.80 were considered substantial; 0.41–0.60 moderate; 0.21–0.40 fair; and 0.00–0.20 as slight agreement.<sup>[75]</sup> Related results are listed in Table 4.

Garcia-Olivé *et al.* also studied reviewer's diagnosis on malignant or not, with  $k$  values of 0.555 and 0.337 for intra- and inter-rater agreement, respectively.<sup>[76]</sup> Schmid-Bindert found that  $k$  values were 0.978 for CHS with blood vessels, 0.978 for CHS without blood vessels, and 0.800 for color power Doppler index.<sup>[26]</sup> In Shafiek's study, the inter-rater agreement (IRA) reached 80% was defined as good, and IRA for hyperechogenic density in the interior of the LN was 81.6%.<sup>[19]</sup> Nakajima *et al.* evaluated blood flow videos and the final results were determined by consensus of at least two reviewers of three reviewers. The intraobserver agreement was 0.830–0.853, and the interobserver agreement was 0.83, indicating good consistency in the evaluation of blood flow videos.<sup>[29]</sup> de Melo *et al.* studied the endosonographic features of LNs in aerodigestive malignancies, and three experts independently evaluated three variables. Shape had a fair interobserver agreement with  $k$  value of 0.35, and echogenicity and margin had moderate interobserver agreement, with  $k$  values of 0.46 and 0.43, respectively.<sup>[77]</sup> Wang *et al.* found that the intraobserver consistency was 0.93 and 0.92, and the interobserver consistency was 0.84 and 0.87 for clustered formation and nonhilar perfusion of vascular pattern, respectively.<sup>[22]</sup>

## DISCUSSION

EBUS imaging plays an important role in the diagnosis

**Table 4. Studies about intra- and interobserver agreement on gray scale sonographic features**

Study	Observers	Short axis >10 mm	Present of CNS	Round shape	Absent of CHS	Heterogeneous echogenicity	Distinct margin	Present of calcification
Intraobserver								
Garcia-Olivé <i>et al.</i> <sup>[76]</sup>	8	0.826	0.721	0.615	0.565	0.441	0.407	\
Wang <i>et al.</i> <sup>[22]</sup>	2	\	0.920	\	0.910	0.910	0.870	0.850
Interobserver								
Garcia-Olivé <i>et al.</i> <sup>[76]</sup>	8	0.641	0.340	0.445	\	\	0.274	\
Schmid-Bindert <i>et al.</i> <sup>[26]</sup>	2	\	\	0.992	\	0.896	0.886	\
Shafiek <i>et al.</i> <sup>[19]</sup>	2	0.860	\	0.910	0.872	0.922	0.915	\
Wang <i>et al.</i> <sup>[22]</sup>	2	\	0.870	\	0.850	0.890	0.830	0.820
Alici <i>et al.</i> <sup>[17]</sup>	3	1.000	1.000	1.000	0.950	1.000	1.000	0.970
Evison <i>et al.</i> <sup>[20]</sup>	2	\	0.830	0.850	0.890	0.860	0.400	\

CHS: Central hilar structure; CNS: Coagulation necrosis sign

of intrathoracic benign and malignant LNs. In lung cancer workup, PET-CT is routinely recommended before intended curative treatment to identify metastasis of LNs. However, PET-CT may have false-positive and false-negative results in the diagnosis of LNs. In recent years, EBUS imaging begins to play an important role in the diagnosis of intrathoracic LNs due to its unique image-forming principle and rapid development. EBUS sonographic features can help bronchoscopist to judge malignant and benign LNs based on CT or PET-CT and may also supplement the false diagnosis. However, at present, there is no study comparing the diagnostic value of PET-CT and EBUS sonographic features.

In clinical operation, for gray scale mode, shape, margin, echo homogeneity, and CNS can be chosen.<sup>[12]</sup> For blood flow Doppler, distribution of blood flow can be chosen, and for elastography, the five-score method studied by Sun *et al.* can be chosen.<sup>[13,54]</sup> For quantitative methods, there are many kinds of elastography quantitative methods, and it is difficult to draw a unified cutoff value for each indicator. Even for the same indicator such as strain ratio (SR), differences between the cutoff values are quite large.<sup>[50,51]</sup> With respect to the interobserver agreement, it can reduce the subjective differences of qualitative results, and k values in most studies can reach to 0.81–1.0 which belongs to perfect agreement except Garcia-Olive *et al.*<sup>[76]</sup>

Previous studies, mainly retrospective, analyzed sonographic factors to find features and combinations with the best diagnostic performance, but there have been few prospective validations of predictive tools. Besides, although many studies found that the diagnostic value of elastography is better than qualitative gray scale, the diagnostic performance of elastography combined with gray scale is superior

reported by Fujiwara *et al.*<sup>[74]</sup> Features coming from different modes can supplement each other to make up disadvantages of a single mode. However, there has not been any research on the combination of three EBUS modes. Combining the optimal evaluation methods of the three modes to construct a comprehensive evaluation tool, and prospectively verify its diagnostic efficacy, is an important area for future research. In addition, the application scope of many results is limited by the inclusion criteria, such as the exclusion of benign diseases from the study that patients with lung cancer staging. Multicenter studies without limiting the types of diseases are necessary to overcome bias caused by distributional difference of patients among different hospitals. Therefore, multicenter prospective studies that do not limit the types of diseases are required.

The evaluation of sonographic features by people is subjective. With the development of artificial intelligence (AI), application of AI to EBUS imaging field may acquire better effect. Tagaya *et al.* used back-propagation algorithms to construct an artificial neural network (ANN) model for the diagnosis of benign and malignant LNs. The diagnostic accuracy of ANNs was 91%, better than 78% and 51% of surgeons with 5 years and 1 year of experience, respectively.<sup>[78]</sup> Although quantitative methods can reduce subjective bias, the analyzed pictures are still derived from manual selection. Video-based deep learning methods can eliminate subjective factors and automatically select representative images from dynamic videos for feature extraction and picture classification. We have designed an automatic image selection model based on deep learning, followed by application of the transfer learning and multitask learning methods to classify pictures [Figure 5]. AI has been widely studied in other fields

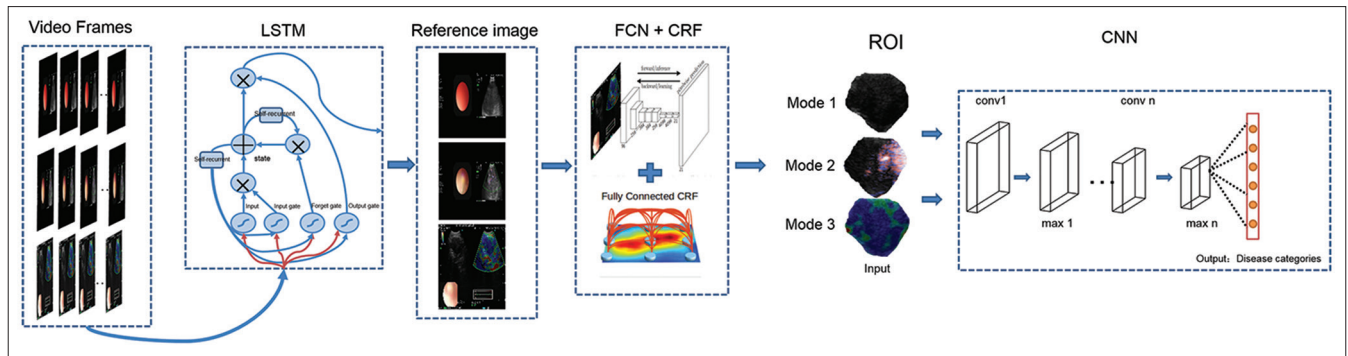


**Figure 5.** Diagram of EBUS multimodal image prediction model based on deep learning. Frames extracted from three modes of EBUS videos are input into the LSTM model, which can build the relationship between frames. With the relation between frames, we can obtain the importance of each frame and select the typical frame from the whole video. ROI is delineated to obtain the lymph node area from the whole image using FCN and CRF. Then, ROI images from three modes are input into CNN under a multi-modal manner which can facilitate the diagnosis of the CNN model. EBUS: Endobronchial ultrasound; LSTM: Long-short term memory; FCN: Fully connected network; CRF: Conditional random field; ROI: Region of interest; CNN: Convolutional neural networks

such as gastrointestinal, breast, and head and neck pathology previously.<sup>[79,80]</sup> In the future, the combination of EBUS image and AI is worthy of further research.

EBUS sonographic features have been widely studied in intrathoracic LNs, but relatively rarely in central lung lesions. It is unknown whether the EBUS assessment criteria for lesions are consistent with LNs. Previous studies reported transthoracic ultrasound elastography in subpleural tumors,<sup>[81]</sup> but there is only one study about EBUS elastography and gray scale features of central lung lesions.<sup>[53]</sup> Therefore, the exploration of EBUS features in lung lesions is a direction worth studying.

## CONCLUSION

EBUS sonographic factors of gray scale, blood flow Doppler, and elastography can be used to predict malignant and benign diagnosis of intrathoracic LNs, but no treatment can be started based on ultrasonographic features and tissue samples should still be obtained to confirm a diagnosis. There are multiple analysis methods, but lack of a universal methods combining the three ultrasound modes. A multi-center prospective verification of a comprehensive model, and the combination of EBUS imaging with AI, will be worthy to study in the future.

### Financial support and sponsorship

This work was supported by the National Natural Science Foundation of China (grant number 81870078), the Shanghai Municipal Health and Medical Talents Training Program (grant number 2018BR09), and the Shanghai Municipal Education Commission-Gaofeng Clinical Medicine Grant Support (grant number 20181815).

### Conflicts of interest

There are no conflicts of interest.

## REFERENCES

1. Yasufuku K, Nakajima T, Fujiwara T, et al. Role of endobronchial ultrasound-guided transbronchial needle aspiration in the management of lung cancer. *Gen Thorac Cardiovasc Surg* 2008;56:268-76.
2. Krasnik M, Vilmann P, Larsen SS, et al. Preliminary experience with a new method of endoscopic transbronchial real time ultrasound guided biopsy for diagnosis of mediastinal and hilar lesions. *Thorax* 2003;58:1083-6.
3. Silvestri GA, Gonzalez AV, Jantz MA, et al. Methods for staging non-small cell lung cancer: Diagnosis and management of lung cancer, 3<sup>rd</sup> ed: American College of Chest Physicians evidence-based clinical practice guidelines. *Chest* 2013;143:e211S-50S.
4. Gamliel Z. Mediastinal staging in non-small cell lung cancer. *Surg Oncol Clin N Am* 2016;25:493-502.
5. Yang H, Wang S, Teng J, et al. Utility of endobronchial ultrasound-guided transbronchial needle aspiration in diagnosing non-specific inflammatory intrathoracic lymphadenitis. *Clin Respir J* 2018;12:691-8.
6. Sun J, Yang H, Teng J, et al. Determining factors in diagnosing pulmonary sarcoidosis by endobronchial ultrasound-guided transbronchial needle aspiration. *Ann Thorac Surg* 2015;99:441-5.
7. Wahidi MM, Herth F, Yasufuku K, et al. Technical aspects of endobronchial ultrasound-guided transbronchial needle aspiration: CHEST guideline and expert panel report. *Chest* 2016;149:816-35.
8. Ying M, Ahuja AT, Yuen HY. Grey-scale and power Doppler sonography of unusual cervical lymphadenopathy. *Ultrasound Med Biol* 2004;30:449-54.
9. Gogia P, Insaf TZ, McNulty W, et al. Endobronchial ultrasound: Morphological predictors of benign disease. *ERJ Open Res* 2016;2:00053-2015.
10. Wang Memoli JS, El-Bayoumi E, Pastis NJ, et al. Using endobronchial ultrasound features to predict lymph node metastasis in patients with lung cancer. *Chest* 2011;140:1550-6.
11. Lin CK, Chang LY, Yu KL, et al. Differentiating metastatic lymph nodes in lung cancer patients based on endobronchial ultrasonography features. *Med Ultrason* 2018;20:154-8.
12. Fujiwara T, Yasufuku K, Nakajima T, et al. The utility of sonographic features during endobronchial ultrasound-guided transbronchial needle aspiration for lymph node staging in patients with lung cancer: A standard endobronchial ultrasound image classification system. *Chest* 2010;138:641-7.
13. Wang L, Wu W, Hu Y, et al. Sonographic features of endobronchial ultrasonography predict intrathoracic lymph node metastasis in lung

- cancer patients. *Ann Thorac Surg* 2015;100:1203-9.
14. Imai N, Imaizumi K, Ando M, et al. Echoic features of lymph nodes with sarcoidosis determined by endobronchial ultrasound. *Intern Med* 2013;52:1473-8.
  15. Dhooria S, Agarwal R, Aggarwal AN, et al. Differentiating tuberculosis from sarcoidosis by sonographic characteristics of lymph nodes on endobronchial ultrasonography: A study of 165 patients. *J Thorac Cardiovasc Surg* 2014;148:662-7.
  16. Gill KR, Ghabril MS, Jamil LH, et al. Endosonographic features predictive of malignancy in mediastinal lymph nodes in patients with lung cancer. *Gastrointest Endosc* 2010;72:265-71.
  17. Alici IO, Yilmaz Demirci N, Yilmaz A, et al. The sonographic features of malignant mediastinal lymph nodes and a proposal for an algorithmic approach for sampling during endobronchial ultrasound. *Clin Respir J* 2016;10:606-13.
  18. Lin CK, Yu KL, Chang LY, et al. Differentiating malignant and benign lymph nodes using endobronchial ultrasound elastography. *J Formos Med Assoc* 2019;118:436-43.
  19. Shafiek H, Fiorentino F, Peralta AD, et al. Real-time prediction of mediastinal lymph node malignancy by endobronchial ultrasound. *Arch Bronconeumol* 2014;50:228-34.
  20. Evison M, Morris J, Martin J, et al. Nodal staging in lung cancer: A risk stratification model for lymph nodes classified as negative by EBUS-TBNA. *J Thorac Oncol* 2015;10:126-33.
  21. Ayub II, Mohan A, Madan K, et al. Identification of specific EBUS sonographic characteristics for predicting benign mediastinal lymph nodes. *Clin Respir J* 2018;12:681-90.
  22. Wang L, Wu W, Teng J, et al. Sonographic features of endobronchial ultrasound in differentiation of benign lymph nodes. *Ultrasound Med Biol* 2016;42:2785-93.
  23. Ahuja AT, Ying M, Ho SY, et al. Ultrasound of malignant cervical lymph nodes. *Cancer Imaging* 2008;8:48-56.
  24. Roberts SA, Mahon BS, Evans R. Coagulation necrosis in malignant mediastinal nodes on endoscopic ultrasound: A new endosonographic sign. *Clin Radiol* 2005;60:587-91.
  25. Michail G, Karahaliou A, Skiadopoulou S, et al. Texture analysis of perimenopausal and post-menopausal endometrial tissue in grayscale transvaginal ultrasonography. *Br J Radiol* 2007;80:609-16.
  26. Schmid-Bindert G, Jiang H, Kähler G, et al. Predicting malignancy in mediastinal lymph nodes by endobronchial ultrasound: A new ultrasound scoring system. *Respirology* 2012;17:1190-8.
  27. Wang Y, Dan HJ, Fan JH, et al. Evaluation of the correlation between colour power Doppler flow imaging and vascular endothelial growth factor in breast cancer. *J Int Med Res* 2010;38:1077-83.
  28. Na DG, Lim HK, Byun HS, et al. Differential diagnosis of cervical lymphadenopathy: Usefulness of color Doppler sonography. *AJR Am J Roentgenol* 1997;168:1311-6.
  29. Nakajima T, Anayama T, Shingyoji M, et al. Vascular image patterns of lymph nodes for the prediction of metastatic disease during EBUS-TBNA for mediastinal staging of lung cancer. *J Thorac Oncol* 2012;7:1009-14.
  30. Zhou J, Zhu SY, Liu RC, et al. Vascularity index of laryngeal cancer derived from 3-D ultrasound: A predicting factor for the *in vivo* assessment of cervical lymph node status. *Ultrasound Med Biol* 2009;35:1596-600.
  31. Lee JH, Shin HJ, Yoon JH, et al. Predicting lymph node metastasis in patients with papillary thyroid carcinoma by vascular index on power Doppler ultrasound. *Head Neck* 2017;39:334-40.
  32. Kagawa T, Yuasa K, Fukunari F, et al. Quantitative evaluation of vascularity within cervical lymph nodes using Doppler ultrasound in patients with oral cancer: Relation to lymph node size. *Dentomaxillofac Radiol* 2011;40:415-21.
  33. Ophir J, Céspedes I, Ponnekanti H, et al. Elastography: A quantitative method for imaging the elasticity of biological tissues. *Ultrasound Imaging* 1991;13:111-34.
  34. Ophir J, Garra B, Kallel F, et al. Elastographic imaging. *Ultrasound Med Biol* 2000;26 Suppl 1:S23-9.
  35. Zaleska-Dorobisz U, Kaczorowski K, Pawluś A, et al. Ultrasound elastography - Review of techniques and its clinical applications. *Adv Clin Exp Med* 2014;23:645-55.
  36. Garra BS, Céspedes EI, Ophir J, et al. Elastography of breast lesions: Initial clinical results. *Radiology* 1997;202:79-86.
  37. Cochlin DL, Ganatra RH, Griffiths DF. Elastography in the detection of prostatic cancer. *Clin Radiol* 2002;57:1014-20.
  38. Lyshchik A, Higashi T, Asato R, et al. Thyroid gland tumor diagnosis at US elastography. *Radiology* 2005;237:202-11.
  39. Nemakayala D, Patel P, Rahimi E, et al. Use of quantitative endoscopic ultrasound elastography for diagnosis of pancreatic neuroendocrine tumors. *Endosc Ultrasound* 2016;5:342-5.
  40. Sandrin L, Fourquet B, Hasquenoph JM, et al. Transient elastography: A new noninvasive method for assessment of hepatic fibrosis. *Ultrasound Med Biol* 2003;29:1705-13.
  41. Okasha HH, Mansour M, Attia KA, et al. Role of high resolution ultrasound/endosonography and elastography in predicting lymph node malignancy. *Endosc Ultrasound* 2014;3:58-62.
  42. Sivokozov IV, Silina TL, Korolev VN, et al. The first experience in using elastography in combination with endobronchial ultrasonography for mediastinal pathology: Preliminary assessment of feasibility and comparison of characteristics via different approaches. *Vestn Rentgenol Radiol* 2014;4:13-9.
  43. Dietrich CF, Jenssen C, Herth FJ. Endobronchial ultrasound elastography. *Endosc Ultrasound* 2016;5:233-8.
  44. Krouskop TA, Wheeler TM, Kallel F, et al. Elastic moduli of breast and prostate tissues under compression. *Ultrasound Imaging* 1998;20:260-74.
  45. Izumo T, Sasada S, Chavez C, et al. Endobronchial ultrasound elastography in the diagnosis of mediastinal and hilar lymph nodes. *Jpn J Clin Oncol* 2014;44:956-62.
  46. Huang H, Huang Z, Wang Q, et al. Effectiveness of the benign and malignant diagnosis of mediastinal and hilar lymph nodes by endobronchial ultrasound elastography. *J Cancer* 2017;8:1843-8.
  47. Gu Y, Shi H, Su C, et al. The role of endobronchial ultrasound elastography in the diagnosis of mediastinal and hilar lymph nodes. *Oncotarget* 2017;8:89194-202.
  48. Korrungruang P, Boonsarngsuk V. Diagnostic value of endobronchial ultrasound elastography for the differentiation of benign and malignant intrathoracic lymph nodes. *Respirology* 2017;22:972-7.
  49. Fournier C, Dhalluin X, Wallyn F, et al. Performance of endobronchial ultrasound elastography in the differentiation of malignant and benign mediastinal lymph nodes: Results in real-life practice. *J Bronchology Interv Pulmonol* 2019;26:193-8.
  50. Hernández Roca M, Pérez Pallarés J, Prieto Merino D, et al. Diagnostic value of elastography and endobronchial ultrasound in the study of hilar and mediastinal lymph nodes. *J Bronchology Interv Pulmonol* 2019;26:184-92.
  51. He HY, Huang M, Zhu J, et al. Endobronchial ultrasound elastography for diagnosing mediastinal and hilar lymph nodes. *Chin Med J (Engl)* 2015;128:2720-5.
  52. Furukawa MK, Kubota A, Hanamura H, et al. Clinical application of real-time tissue elastography to head and neck cancer-evaluation of cervical lymph node metastasis with real-time tissue elastography. *Nihon Jibiinkoka Gakkai Kaiho* 2007;110:503-5.
  53. He HY, Chen JL, Ma H, et al. Value of endobronchial ultrasound elastography in diagnosis of central lung lesions. *Med Sci Monit* 2017;23:3269-75.
  54. Sun J, Zheng X, Mao X, et al. Endobronchial ultrasound elastography for evaluation of intrathoracic lymph nodes: A pilot study. *Respiration* 2017;93:327-38.
  55. Săftoiu A, Vilmann P, Hassan H, et al. Analysis of endoscopic ultrasound elastography used for characterisation and differentiation of benign and malignant lymph nodes. *Ultraschall Med* 2006;27:535-42.
  56. Verhoeven RL, de Korte CL, van der Heijden E. Optimal endobronchial ultrasound strain elastography assessment strategy: An explorative study. *Respiration* 2019;97:337-47.
  57. Giovannini M, Thomas B, Erwan B, et al. Endoscopic ultrasound elastography for evaluation of lymph nodes and pancreatic masses: A multicenter study. *World J Gastroenterol* 2009;15:1587-93.

58. Trosini-Désert V, Jeny F, Maksud P, et al. Contribution of endobronchial ultrasound elastography to the characterization of mediastinal lymphadenopathy: A single-center, prospective, observational study. *Respir Med Res* 2019;76:28-33.
59. Rozman A, Malovrh MM, Adamic K, et al. Endobronchial ultrasound elastography strain ratio for mediastinal lymph node diagnosis. *Radiol Oncol* 2015;49:334-40.
60. Hernández Roca M, Pérez Pallarés J, Valdivia Salas MD, et al. Endobronchial ultrasound elastography for diagnosing mediastinal and hilar lymph nodes. *Med Clin (Barc)* 2020;154:45-51.
61. Abedini A, Razavi F, Farahani M, et al. The utility of elastography during EBUS-TBNA in a population with a high prevalence of anthracosis. *Clin Respir J* 2020;14:488-94.
62. Nakajima T, Inage T, Sata Y, et al. Elastography for predicting and localizing nodal metastases during endobronchial ultrasound. *Respiration* 2015;90:499-506.
63. Ma H, An Z, Xia P, et al. Semi-quantitative analysis of EBUS elastography as a feasible approach in diagnosing mediastinal and hilar lymph nodes of lung cancer patients. *Sci Rep* 2018;8:3571.
64. Mao XW, Yang JY, Zheng XX, et al. Comparison of two quantitative methods of endobronchial ultrasound real-time elastography for evaluating intrathoracic lymph nodes. *Zhonghua Jie He He Hu Xi Za Zhi* 2017;40:431-4.
65. Cui XW, Chang JM, Kan QC, et al. Endoscopic ultrasound elastography: Current status and future perspectives. *World J Gastroenterol* 2015;21:13212-24.
66. Landoni V, Francione V, Marzi S, et al. Quantitative analysis of elastography images in the detection of breast cancer. *Eur J Radiol* 2012;81:1527-31.
67. Săftoiu A, Vilmann P, Ciurea T, et al. Dynamic analysis of EUS used for the differentiation of benign and malignant lymph nodes. *Gastrointest Endosc* 2007;66:291-300.
68. Săftoiu A, Vilmann P, Gorunescu F, et al. Neural network analysis of dynamic sequences of EUS elastography used for the differential diagnosis of chronic pancreatitis and pancreatic cancer. *Gastrointest Endosc* 2008;68:1086-94.
69. Shiina Y, Nakajima T, Suzuki H, et al. Localization of the metastatic site within a lymph node using endobronchial elastography. *Semin Thorac Cardiovasc Surg* 2019;31:312-4.
70. Zarogoulidis P, Kosmidis C, Fyntanidou V, et al. Elastography during convex-probe (endobronchial ultrasound) for optimal biopsy sample and gene identification in non-small-cell lung cancer. *Biomark Med* 2019;13:1153-6.
71. Livi V, Cancellieri A, Pirina P, et al. Endobronchial ultrasound elastography helps identify fibrotic lymph nodes in sarcoidosis. *Am J Respir Crit Care Med* 2019;199:e24-5.
72. Săftoiu A, Vilmann P, Gorunescu F, et al. Efficacy of an artificial neural network-based approach to endoscopic ultrasound elastography in diagnosis of focal pancreatic masses. *Clin Gastroenterol Hepatol* 2012;10:84-90.
73. Akissue de Camargo Teixeira P, Chala LF, Shimizu C, et al. Axillary lymph node sonographic features and breast tumor characteristics as predictors of malignancy: A nomogram to predict risk. *Ultrasound Med Biol* 2017;43:1837-45.
74. Fujiwara T, Nakajima T, Inage T, et al. The combination of endobronchial elastography and sonographic findings during endobronchial ultrasound-guided transbronchial needle aspiration for predicting nodal metastasis. *Thorac Cancer* 2019;10:2000-5.
75. Landis JR, Koch GG. The measurement of observer agreement for categorical data. *Biometrics* 1977;33:159-74.
76. Garcia-Olivé I, Radua J, Serra P, et al. Intra- and interobserver agreement among bronchial endosonographers for the description of intrathoracic lymph nodes. *Ultrasound Med Biol* 2012;38:1163-8.
77. de Melo SW, Jr., Panjala C, Crespo S, et al. Interobserver agreement on the endosonographic features of lymph nodes in aerodigestive malignancies. *Dig Dis Sci* 2011;56:3204-8.
78. Tagaya R, Kurimoto N, Osada H, et al. Automatic objective diagnosis of lymph nodal disease by B-mode images from convex-type echobronchoscopy. *Chest* 2008;133:137-42.
79. Min JK, Kwak MS, Cha JM. Overview of deep learning in gastrointestinal endoscopy. *Gut Liver* 2019;13:388-93.
80. Wu GG, Zhou LQ, Xu JW, et al. Artificial intelligence in breast ultrasound. *World J Radiol* 2019;11:19-26.
81. Sperandeo M, Trovato FM, Dimitri L, et al. Lung transthoracic ultrasound elastography imaging and guided biopsies of subpleural cancer: A preliminary report. *Acta Radiol* 2015;56:798-805.